One-minute synthesis of crystalline binary and ternary metal oxide nanoparticles†

Idalia Bilecka, Igor Djerdj and Markus Niederberger*

Received (in Cambridge, UK) 9th November 2007, Accepted 6th December 2007
First published as an Advance Article on the web 19th December 2007
DOI: 10.1039/b717334b

Highly crystalline metal oxide nanoparticles such as CoO, ZnO, Fe_3O_4, MnO, Mn_3O_4, and $BaTiO_3$ were synthesized in just a few minutes by reacting metal alkoxides, acetates or acetylacetonates with benzyl alcohol under microwave heating.

Metal oxide nanoparticles constitute an outstanding class of functional materials with potential applications in almost all fields of technology.[1] Among the different synthesis approaches developed in the last few years, nonaqueous or nonhydrolytic processes were particularly successful with respect to achieving control of crystallite size, shape, and assembly behavior.[2–5] But in spite of all the progress, the preparation of nanocrystalline metal oxides remains rather time- and also energy-consuming. One possibility to accelerate the synthesis process is the use of microwave irradiation, which allows a more efficient and homogeneous heating of the reaction mixture. Microwave-assisted preparation routes for inorganic materials are not yet as popular as for organic compounds. However, the growing number of publications dealing with that topic gives a first impression about the great potential of the method.[6–8] The composition of inorganic nanoparticles obtained *via* microwave heating ranges from metals (Au, Pd, Ag, Pt, AuPb)[8,9] to oxides (TiO_2, $BaTiO_3$, tungstates, ZnO),[10–15] chalcogenides [M_2S_3 (M = Bi, Sb), ZnS, ZnSe, CdSe, PbTe, PbSe, CdS],[16–19] and phosphates ($LaPO_4$:Ce,Tb)[20] and the solvents used include water, organic solvents, or ionic liquids.

Here we present a broadly applicable synthesis strategy that enables the preparation of highly crystalline metal oxide nanoparticles in good yields within minutes and even seconds using a combination of nonaqueous sol–gel chemistry and microwave heating. Thus, the use of microwave heating offers an immense reduction of the reaction times in comparison to traditional heating in an oil bath or in an autoclave. Furthermore, the pronounced dependence of the crystallite size on the heating time (which was not found in analogous solvothermal experiments in the autoclave[21–23]) provides a precious tool to tailor this parameter. Comparison of the reaction mechanism of ZnO, prepared either in the microwave or in the autoclave, proved that both processes involved ester elimination as condensation step for the Zn–O–Zn bond formation. This result is of utmost significance, because it gives strong indication that microwave irradiation can be used as a powerful tool to accelerate the formation of metal oxide nanoparticles through directly influencing the organic reaction pathways.

The synthesis of the metal oxide nanoparticles involved the dispersion of the precursors in benzyl alcohol (Scheme 1), followed by heating in a microwave of 2.45 GHz frequency, with the power modulated as a function of temperature (for details see ESI†). The reaction mixture was continuously stirred and then thermally quenched by a compressed air jet. The temperature profile during the reaction can be divided into three regions (see ESI†) that all play an important role for nanoparticle formation. In the first stage, the mixture is heated from room temperature to 60 °C to allow the precursor to completely dissolve. Thereafter, fast heating to 200 °C leads to homogeneous nucleation, probably following the same model as recently reported for the preparation of monodisperse iron oxide nanocrystals by a heating-up process.[24] Crystal growth occurred then upon further heating at this temperature, enabling control over the final crystallite size.

Powder X-ray diffraction (XRD) patterns of the obtained samples (Cu Kα or Co Kα radiation) are shown in Fig. 1. All patterns correspond to the respective phase-pure metal oxide with broad reflections that point to nanosized crystallites. The XRD pattern of the brownish CoO sample can be assigned to the cubic rocksalt-type phase (ICDD PDF No. 01-089-7099) with a crystallite size of 6 nm calculated by Scherrer analysis of the 200 reflection (Fig. 1a). In the case of ZnO (Fig. 1b), independent of the precursor $Zn(ac)_2$ or $Zn(acac)_2$ the final white powder consisted of zincite ZnO (ICDD PDF No. 36-1451). However, according to Scherrer analysis of the 100 reflection the crystallite size amounted to 20 nm for the acetylacetonate as precursor, whereas for the acetate the sizes are in general larger (around 25–30 nm). The reaction of

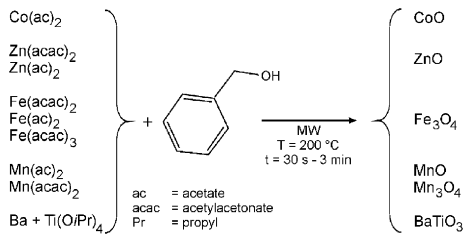

Scheme 1 General reaction scheme displaying the metal oxide precursors used, the solvent, the experimental conditions, and the resulting metal oxide nanoparticles.

Laboratory for Multifunctional Materials, Department of Materials, ETH Zürich, Wolfgang-Pauli Strasse 10, 8093 Zürich, Switzerland. E-mail: markus.niederberger@mat.ethz.ch; Fax: 41 44 632 11 01; Tel: 41 44 633 63 90

† Electronic supplementary information (ESI) available: experimental details, temperature/pressure profile, XRD powder pattern of MnO and Mn_3O_4, TEM images of ZnO. See DOI: 10.1039/b717334b

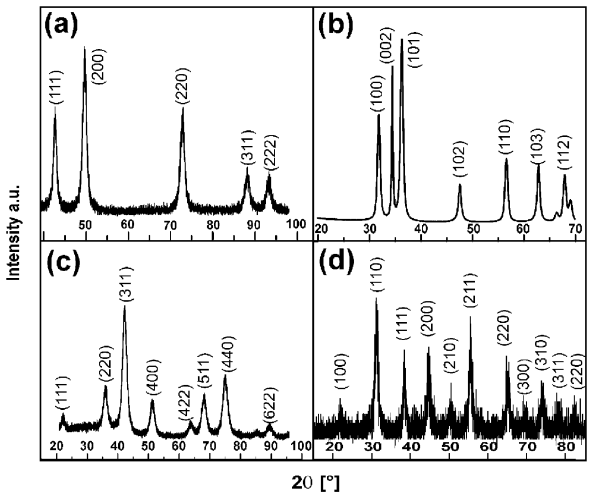

Fig. 1 X-ray diffraction patterns of (a) CoO, (b) ZnO, (c) Fe_3O_4, and (d) $BaTiO_3$ (a) and (c) Co Kα, (b) and (d) Cu Kα radiation.

$Fe(ac)_2$, $Fe(acac)_2$ or $Fe(acac)_3$ yielded black powders that showed magnetic behavior under the influence of a permanent magnet. Although the XRD powder patterns were similar for all three samples (Fig. 1c) and could clearly be assigned to magnetite Fe_3O_4 (ICDD PDF No. 19-629), their crystallite sizes (extracted from the 311 reflection) differed considerably in dependence of the precursor used. 11 nm-sized crystals were obtained with $Fe(acac)_2$, 7 nm with $Fe(ac)_2$ and $Fe(acac)_3$ gave the smallest crystallites of just 5 nm. In the case of the manganese oxide nanoparticles, the choice of the precursor does not only influence the crystallite size, but the final phase composition (see ESI†). $Mn(ac)_2$ favoured the formation of 10 nm sized MnO (calculated from the 200 reflection) in the manganosite structure (ICDD PDF No. 7-230), wheras $Mn(acac)_2$ resulted in 7 nm sized (from the 224 reflection) Mn_3O_4 hausmannite (ICDD PDF No. 24-734). The XRD pattern in Fig. 1d corresponds to $BaTiO_3$ (ICDD PDF No. 31-174). In this case it is worth highlighting again that there is no indication of $BaCO_3$ as crystalline by-product. The crystallite size extracted from the (110) reflection amounts to about 12 nm. Due to the small crystal size the reflections are too broad to discriminate between the cubic and the tetragonal structure.[23]

Representative transmission electron microscopy (TEM) images were used to study the particle morphologies and size distributions (Fig. 2). All the images display well-dispersed nanoparticles, however with different morphologies and varying uniformity. The size and shape of the CoO (Fig. 2a) and ZnO (see ESI†) nanoparticles is not very well defined, but roughly agrees with the XRD data. On the other hand, MnO is characterized by a relatively homogeneous cube-like shape (Fig. 2b). The side lengths of these cubes (30–50 nm) is considerably larger than the crystallite size measured by XRD, which points to a polycrystalline nature of these particles. The magnetite sample in Fig. 2c [prepared from $Fe(ac)_2$] exhibits a rather uniform spherical particle morphology with a small size distribution in the range of 5 to 10 nm, which agrees well with XRD data. The $BaTiO_3$ nanoparticles are particularly well dispersed, with sizes in the range of

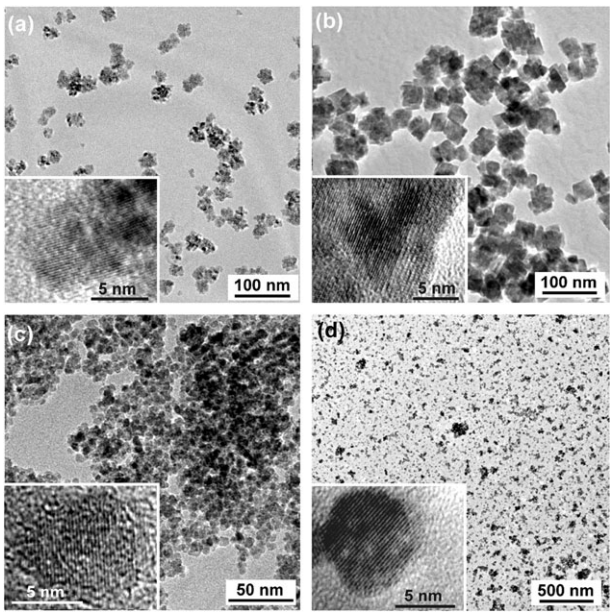

Fig. 2 TEM and HRTEM images (insets) of (a) CoO, (b) MnO, (c) Fe_3O_4, and (d) $BaTiO_3$.

6–18 nm (Fig. 2d), also matching the XRD data. All these metal oxides exhibit well-defined lattice fringes in the corresponding HRTEM images (Fig. 2, insets), proving the high crystallinity of these nanomaterials.

Different organic reaction pathways have been identified to play a crucial role in the nonaqueous liquid-phase synthesis of nanocrystalline metal oxides particles.[4,5] The investigation of the organic reaction mechanism involved in the formation of ZnO starting from $Zn(ac)_2$ provides a unique opportunity to compare the crystallization process of the nanoparticles either under microwave heating (for a few minutes) or in the autoclave (for several hours). Thus, the final reaction solutions after removal of the inorganic precipitates were analyzed by coupled gas-chromatography–mass spectrometry (GC-MS). In addition to the solvent benzyl alcohol, the only organic species detected was benzyl acetate. Based on this result, one can clearly state that autoclave as well as microwave heating led to ZnO formation *via* an ester elimination process.[25] At this point, we can only speculate about the underlying effect, which results in the great acceleration of the microwave heating process in comparison to the autoclave synthesis. In general, the acceleration of reactions by microwave exposure is due to thermal effects (dielectric heating) and specific nonthermal effects.[26] Decrease in the activation energy is the most important part of the specific nonthermal microwave effect, which is a consequence of the greater stabilization of the transition state during the reaction course compared to the ground state.[26] The effect is particularly pronounced, when the transition state is more polar than the ground state, *i.e.*, when the dipole moment is enhanced from the ground to the transition state.[26] Considering that the formation of benzyl acetate by nucleophilic attack on the acetate ligand proceeds *via* a highly polar transition state, the acceleration can be explained on the basis of the specific nonthermal microwave effect.

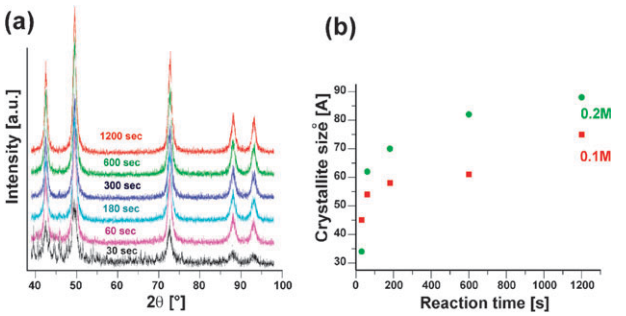

Fig. 3 (a) X-ray diffraction pattern (using Co Kα radiation) of CoO obtained after reaction times ranging from 30 s to 20 min (0.1 M precursor concentration). (b) Evolution of the average crystallite size (calculated from the 200 reflection) with the reaction time and in dependence of the precursor concentration.

Table 1 Crystallite sizes of CoO nanoparticles calculated by Scherrer analysis of the 200 reflection in dependence of the heating time (0.1 M precursor concentration)

Sample no	Thermal treatment/s	XRD particle size/Å	Reaction yield [%]
1	30	45	60.8
2	60	54	68.8
3	180	58	66.2
4	600	61	70
5	1200	75	77

In the solvothermal nonaqueous sol–gel synthesis of metal oxide nanoparticles in benzyl alcohol, especially the choice of the precursor influences the final crystal size, morphology, and composition.[4,5] Parameters like reaction time and precursor concentration just play a minor role. However, in the case of microwave heating these parameters become more important. Therefore, time dependant studies in the CoO system were performed using two different precursor concentrations. XRD analysis (Fig. 3a) of the CoO samples obtained after different reaction times in the range of 30 s to 20 min revealed that already after 30 s the main reflections of CoO are present, in addition to other not yet assignable peaks. After one minute, the CoO sample is phase-pure and longer heat treatment just results in crystallite growth from about 5 to 8 nm, which can easily be monitored by the narrowing of the 200 reflection (Table 1). Furthermore, at the same temperature the yield increases with reaction time from about 60% to nearly 80%. Enhanced crystal growth cannot only be achieved by extending the heating time, but also by increasing the precursor concentration from 0.1 to 0.2 M (Fig. 3b). The crystallite sizes change then from about 3 to 9 nm as the reaction time increases. A closer look at the two curves in Fig. 3b shows two distinct kinetic regimes, *i.e.*, during the first minutes the average crystallite size increases rapidly, followed by a slower growth after about 3 min.

The results reported here on the one hand offer a fast synthesis route to a variety of binary and ternary metal oxide nanoparticles with high crystallinity, and on the other hand propose a way to control the reaction rate by applying microwave irradiation to influence (*i.e.*, to accelerate) the organic reaction pathway occurring in parallel to nanoparticle formation. In comparison to the corresponding synthesis procedures performed in the autoclave, the reactions are much faster and the crystallite size is tunable. The fact that nanoparticle formation is based on the same mechanism in the autoclave and in the microwave strongly supports the proposition that microwave irradiation has a great potential to control the growth of inorganic nanoparticles through influencing the organic reaction pathways.

Financial support by the ETH Zürich is gratefully acknowledged. We made use of the facilities provided by EMEZ (Electron Microscopy ETH Zürich).

References

1 J. A. Rodriguez and M. Fernandez-Garcia, *Synthesis, Properties and Applications of Oxide Nanomaterials*, John Wiley & Sons, New Jersey, 2007.
2 Y. W. Jun, J. S. Choi and J. Cheon, *Angew. Chem., Int. Ed.*, 2006, **45**, 3414.
3 J. Park, J. Joo, S. G. Kwon, Y. Jang and T. Hyeon, *Angew. Chem., Int. Ed.*, 2007, **46**, 4630.
4 M. Niederberger and G. Garnweitner, *Chem.–Eur. J.*, 2006, **12**, 7282.
5 M. Niederberger, *Acc. Chem. Res.*, 2007, **40**, 793.
6 D. M. P. Mingos, *Adv. Mater.*, 1993, **5**, 857.
7 K. J. Rao, B. Vaidhyanathan, M. Ganguli and P. A. Ramakrishnan, *Chem. Mater.*, 1999, **11**, 882.
8 M. Tsuji, M. Hashimoto, Y. Nishizawa, M. Kubokawa and T. Tsuji, *Chem.–Eur. J.*, 2005, **11**, 440.
9 F. K. Liu, Y. C. Chang, F. H. Ko and T. C. Chu, *Mater. Lett.*, 2004, **58**, 373.
10 W. W. Wang and Y. J. Zhu, *Inorg. Chem. Commun.*, 2004, **7**, 1003.
11 S. Baldassari, S. Komarneni, E. Mariani and C. Villa, *Mater. Res. Bull.*, 2005, **40**, 2014.
12 A. V. Murugan, V. Samuel and V. Ravi, *Mater. Lett.*, 2006, **60**, 479.
13 K. L. Ding, Z. J. Miao, Z. M. Liu, Z. F. Zhang, B. X. Han, G. M. An, S. D. Miao and Y. Xie, *J. Am. Chem. Soc.*, 2007, **129**, 6362.
14 J. M. Lee, D. P. Amalnerkar, Y. K. Hwang, S. H. Jhung, J. S. Hwang and J. S. Chang, *J. Nanosci. Nanotechnol.*, 2007, **7**, 952.
15 A. Michailovski, R. Kiebach, W. Bensch, J. D. Grunwaldt, A. Baiker, S. Komarneni and G. R. Patzke, *Chem. Mater.*, 2007, **19**, 185.
16 R. Kerner, O. Palchik and A. Gedanken, *Chem. Mater.*, 2001, **13**, 1413.
17 A. B. Panda, G. Glaspell and M. S. El-Shall, *J. Am. Chem. Soc.*, 2006, **128**, 2790.
18 Y. Jiang and Y. J. Zhu, *J. Phys. Chem. B*, 2005, **109**, 4361.
19 A. V. Murugan, R. S. Sonawane, B. B. Kale, S. K. Apte and A. V. Kulkarni, *Mater. Chem. Phys.*, 2001, **71**, 98.
20 G. Buehler and C. Feldmann, *Angew. Chem., Int. Ed.*, 2006, **45**, 4864.
21 N. Pinna, S. Grancharov, P. Beato, P. Bonville, M. Antonietti and M. Niederberger, *Chem. Mater.*, 2005, **17**, 3044.
22 I. Djerdj, D. Arcon, Z. Jaglicic and M. Niederberger, *J. Phys. Chem. C*, 2007, **111**, 3614.
23 M. Niederberger, G. Garnweitner, N. Pinna and M. Antonietti, *J. Am. Chem. Soc.*, 2004, **126**, 9120.
24 S. G. Kwon, Y. Piao, J. Park, S. Angappane, Y. Jo, N.-M. Hwang, J.-G. Park and T. Hyeon, *J. Am. Chem. Soc.*, 2007, **129**, 12571.
25 G. Clavel, M.-G. Willinger, D. Zitoun and N. Pinna, *Adv. Funct. Mater.*, 2007, **17**, 3159.
26 A. Loupy, *Microwaves in Organic Synthesis*, Vol. 1, Wiley-VCH, Weinheim, 2006.

